PAPER

Check for updates

Self-catalyst β-Ga$_2$O$_3$ semiconductor lateral nanowire networks synthesis on the insulating substrate for deep ultraviolet photodetectors†

Yutong Wu, [ID] [ab] Shuanglong Feng, [ID] [bc] Miaomiao Zhang, [bc] Shuai Kang, [ID] [b] Kun Zhang, [ID] [ab] Zhiyong Tao, [d] Yaxian Fan*[d] and Wenqiang Lu [ID] *[bc]

Monoclinic gallium oxide (β-Ga$_2$O$_3$) is a super-wide bandgap semiconductor with excellent chemical and thermal stability, which is an ideal candidate for detecting deep ultraviolet (DUV) radiation (100–280 nm). The growth of β-Ga$_2$O$_3$ is challenging and most methods require Au as the catalyst and a long reacting time (more than 1 hour). In this work, the self-catalyst β-Ga$_2$O$_3$ lateral nanowire networks were synthesized on an insulating substrate rapidly by a simple low-cost Chemical Vapor Deposition (CVD) method. A thin film of β-Ga$_2$O$_3$ nanowire networks was synthesized within a reacting time of 15 minutes, which possesses a huge possibility for the rapid growth of β-Ga$_2$O$_3$ metal oxide nanowires networks and application in the future solar-blind photodetector. MSM (metal–semiconductor–metal) photodetectors based on the β-Ga$_2$O$_3$ nanowire networks revealed fast response (on−off ratios is about 10^3), which is attributed to the unique cross-junction barrier-dominated conductance of the nanowire networks. In addition, the self-catalyst β-Ga$_2$O$_3$ nanowires grown on insulating SiO$_2$ are achieved and could be expected to find important applications in a bottom-up way of fabricating the next generation semiconductor nanoelectronics.

Introduction

Solar-blind deep ultraviolet (DUV) photodetectors, sensitive to a spectrum range from 200 to 280 nm,[1,2] have drawn considerable attention due to their wide applications in commercial and military fields, including flame or engine monitoring, missile warning, chemical or biological agent sensing and ultraviolet (UV) astronomy.[3–8] Compared with thin-film counterparts, high-quality 1D nanostructures that usually have a high specific surface area would raise the density of surface trap states. Also, the low dimensionality could strongly confine the charge carriers, which provide high responsivity and photoconductive gain in nanoscale photodetectors.[9] Inspired by these ideas, various UV light detectors based on 1D semiconductor structures have been fabricated.[10–14]

Monoclinic gallium oxide (β-Ga$_2$O$_3$) is a super-wide bandgap semiconductor (4.9 eV) material with excellent chemical and

thermal stability, which is an ideal candidate for detecting deep ultraviolet (DUV) radiation (200–280 nm).[15] Many works on the optoelectronic properties of β-Ga$_2$O$_3$ single crystal, film and planar heterojunctions have been carried out.[16–23] Their excellent photoelectric properties prove the promising applications of gallium oxide in deep UV detection. Over the last few decades, 1D nanomaterials have attracted intensive fascinating both fundamental science and potential applications in future nanoscale electronics, optoelectronics and sensing devices. Their unique geometry offers fascinating and novel physical properties. Several DUV photodetectors based on β-Ga$_2$O$_3$ in either thin films or nanostructures have been successfully developed.[24–32] In particular, benefiting from quantum confinement effect and remarkable surface/size effect, β-Ga$_2$O$_3$ nanostructures, mainly 1D β-Ga$_2$O$_3$ nanowires (NWs) nanobelts (NBs), can exhibit attractive merits of better optical absorption, improved charge carrier counterpart.[33–38] Therefore, significant progress has been made in the growth of high-quality β-Ga$_2$O$_3$ NWs/NBs for DUV photodetectors' application. Due to a large surface-to-volume ratio and a Debye length comparable to the small size, they demonstrate superior sensitivity to surface processes. Besides, their size confinement renders a tunable bandgap, higher optical gain and faster operation speed.[39–43] Furthermore, the catalysts, such as Au, Pt, Sn, *etc.*, as precious metals catalysts, are usually used in the semiconductor oxide nanowires synthesis process. These catalysts are too expensive and will take metal contamination to the synthesis process. A

[a] *Key Laboratory of In-Fiber Integrated Optics, Ministry Education of China, Harbin Engineering University, Harbin, 150001, PR China*

[b] *Chongqing Key Laboratory of Multi-Scale Manufacturing Technology, Chongqing Institute of Green and Intelligent Technology, Chinese Academy of Sciences, Chongqing, 400714, PR China. E-mail: wqlu@cigit.ac.cn*

[c] *University of Chinese Academy of Sciences, Beijing 100049, China*

[d] *Guangxi Key Laboratory of Wireless Wideband Communication and Signal Processing, Guilin 541004, China. E-mail: yxfan@guet.edu.cn*

† Electronic supplementary information (ESI) available. See DOI: 10.1039/d1ra04663b

simple self-catalyst or without-catalyst semiconductor nanowires synthesis process development is necessary. And also, this self-catalyst synthesis method is conducive to promoting process, which the metal-oxide semiconductor nanowires synthesized on the insulator SiO_2 surface to form semiconductor–insulator nanostructure.[44,45]

This paper proposes a simple and low-cost method of growing the self-catalyst ultra-long β-Ga_2O_3 nanowire networks on SiO_2 insulating substrate using chemical vapor deposition (CVD). Self-catalyst reaction refers to a type of reaction in which the reactant itself has a catalytic effect and can accelerate or slow down the progress of the reaction. Here, Ga metal's catalyst is from reducing the nutrient of β-Ga_2O_3 at the beginning of the synthesis process. In general, the experiments were carried out with the sources of reducing carbon agent that the only commonly used carbon is graphite, which requires a higher heating temperature for thermal reducing and vaporizing the source. Because of all, nano-diamond was used as carbon sources in this work. Compared with other carbon sources, the reaction of nano-diamond as a raw material can reduce the reaction temperature and enhance the intensity of the reaction.[46,47] The response and recovery time of the β-Ga_2O_3 nanowire networks photodetector device under 254 nm DUV light illumination at room temperature are 3.01 s and 0.12 s, respectively current is about 10^3 times higher than the dark current. Finally, we investigated the fast growth principle of the β-Ga_2O_3 nanowire networks and the current transmission in the nanowire networks. Furthermore, this method can be used to sustain metal oxide, and the prepared β-Ga_2O_3 nanowire networks can be applied to DUV detectors were both confirmed. In addition, the self-catalyst Ga_2O_3 nanowires grown on insulating SiO_2 are achieved and could be expected to find important applications in a bottom-up way of fabricating the next generation semiconductor nanoelectronics.

Experiment

The lateral β-Ga_2O_3 nanowire network was grown in a high-temperature tube furnace by chemical vapor deposition (CVD) on the insulating SiO_2/Si substrate. First, Ga_2O_3 nanopowders and nano-diamond powders, mixed as the reaction materials with a mass ratio of 4 : 1 (totally 0.25 g), were placed in a quartz boat. The substrate is placed face up in the center of the quartz boat, as shown in Fig. S1.† Then, the quartz boat with the substrate was pushed into the center of the tube furnace at room temperature, and the tube was pumped to keep the pressure below 1 Pa by using an oil pump. Ar gas was introduced as a carrier gas at a flow rate of 100 sccm, and the gas pressure in the furnace was maintained at 10 kPa by adjusting the size of the suction valve. Simultaneously, a heating program was set and started to make the temperature up in the furnace at 18 °C per minute. When the temperature reaches 1050 °C, oxygen with a flow rate of 1 sccm was passed. The oxygen and argon are turned off immediately while the temperature of the furnace was kept constant for 1 minute, 5 minutes, 15 minutes at 1150 °C, respectively. The white substance obtained on the substrate surface is the β-Ga_2O_3 nanowire network materials.

Photodetector fabrication and characterization

All the as-grown nanowire networks were characterized by field-emission scanning electron microscope (FE-SEM, JEOL7800F), energy dispersive X-ray spectrometer (EDS) (GENESIS 2000 XMS60S), high-resolution transmission electron microscopy (HRTEM, JEM2100 operated at 200 kV, JEOL), X-ray diffractometer (XRD) (Rigaku RINT2500 TRAX-III, Cu Kα radiation) and UV-3101PC scanning spectrophotometer. The current–voltage (I–V) characteristics and photoresponse of the β-Ga_2O_3 photodetectors were measured with a potentiostat (CHI660E, Shanghai Chenhua Instrument). Ultraviolet rays with 245 nm and 365 nm wavelengths were used as illumination sources (UVLS-28EL, Ultra-Violet Products) for the photoresponse measurements. An optical beam shutter (GCI-73, GCI-7103M, Daheng New Epoch Technology) was employed for time-resolved measurements. The optical power density was measured using an optical power meter (S120VC, Thorlabs). All measurements were performed at room temperature.

Results and discussion

Fig. 1 is the characterization of β-Ga_2O_3 nanowire networks. Fig. 1a presents SEM photographs of β-Ga_2O_3 nanowire networks prepared for 15 min at 1150 °C, and the inset is an enlarged image which we can observe the diameter of the nanowire is about 500 nm, the detailed statistics are supplemented in Fig. S2.† Fig. 1b is the EDS spectrum of the nanowire. It further affirms O and Ga elements in the β-Ga_2O_3 nanowires (NWs). The inset plots the absorption spectrum of the β-Ga_2O_3 NWs, which strong absorption at deep ultraviolet with an absorption peak at the wavelength of 249 nm and an absorption
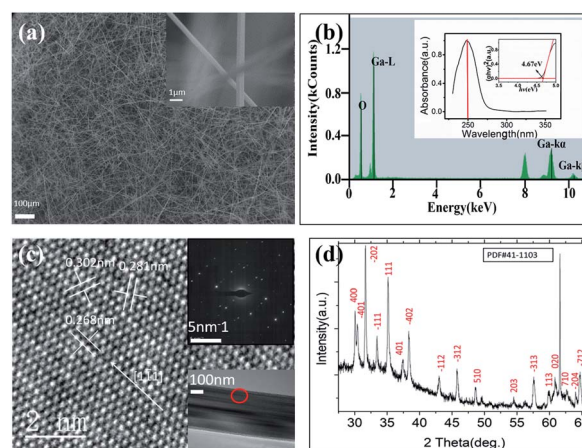

Fig. 1 SEM/XRD/TEM characterization results for the as-synthesized Ga_2O_3 NWs on the SiO_2/Si substrate (a) high magnification SEM image of β-Ga_2O_3 sample grown at 1150 °C, inset is a magnification of nanowire network; (b) the EDS spectrum of the nanowire, inset is the absorption spectrum of the β-Ga_2O_3 nanowire, inset is the plot of $(\alpha h\nu)^2$ versus $h\nu$ that gives the bandgap of β-Ga_2O_3 nanowire; (c) high-resolution TEM image of the single β-Ga_2O_3 nanowire, inset is SAED image; (d) XRD patterns of the single β-Ga_2O_3 nanowire.

edge located at ≈ 275 nm. Besides, by extrapolating the curve of $(\alpha h\nu)^2$–$h\nu$ (where α represents absorbance, h represents Planck's constant, and ν represents frequency)[48] to zero intensity (inset in Fig. 1b), the optical bandgap of the β-Ga_2O_3 NWs is determined to be ≈ 4.67 eV, which coincides with the values in previous reports. The TEM image in Fig. 1c indicates that the nanowire is polycrystalline with lattice spaces of 0.32 and 0.28 nm, which are corresponding to the (400) and ($\bar{1}$11) plane of β-Ga_2O_3, respectively. Fig. 1d shows XRD patterns of the sample, and all the diffraction peaks can be readily indexed within the monoclinic crystalline phase of β-Ga_2O_3. The lattice constants were determined to be $a = 1.223$ nm, $b = 3.039$ nm, $c = 0.581$ nm, and $\beta = 103.8°$, which is in good agreement with the standard values β-Ga_2O_3 (JCPDS card no. 41-1103).[49] According to the TGA data in Fig. S3,† it can be seen that there is basically no organic matter in the nanowire networks. The above results confirm that β-Ga_2O_3 NWs with high-crystalline quality have been successfully synthesized.

Fig. 2 presents SEM photographs of β-Ga_2O_3 nanowire networks prepared of 1 min, 5 min, and 15 min at 1150 °C, respectively. According our experiments data, the nanowire length growth speed is very fast. The nanowires length is measured after it was synthesized in different growth time, such as, 1 minute, 5 minutes, 10 minutes, 15 minutes, 20 minutes. A 2.0 mm nanowire length was achieved at a 30 minutes growth time. The diameter of the nanowire exceeded 1.0 μm when the reaction time exceeds 20 minutes in Fig. S4.† Usually, this kind of over 1.0 μm diameter nanowires is not belong to nanoscale category. So, the nanowires sample with 15 minutes growth time was selected to fabricate the photodetector devices. At the beginning of the reaction, it can be seen from Fig. 1a that irregular gallium suboxide (Ga_2O) particles are deposited on the substrate and the inset is enlarged image of Ga_2O particles.[50] The particle size is about 200 nm. Fig. 2b shows the EDS spectrum of particles that the Gallium is observed clearly. It indicates the VS growth mechanism for the nanowire. The Ga_2O_3 is

reduced by liquid metallic gallium and forms a gas phase of Ga_2O. The Ga_2O gas-phase gets transported to cooler regions and decomposes to liquid gallium and Ga_2O_3, leading to a vapour–solid (VS) growth mechanism. After the reaction for 5 minutes, we could observe some β-Ga_2O_3 NWs sprout from the nuclei and the β-Ga_2O_3 NWs have already contacted with the ones from neighbour pillars and even form some multi-channel junctions, but the β-Ga_2O_3 NWs density is still relatively low with most of the area between substrates uncovered, as indicated in Fig. 2c, the diameter of β-Ga_2O_3 NW is about 100 nm. After a growth time of 15 minutes, the β-Ga_2O_3 NWs covered all the substrates, as indicated in Fig. 2d, the diameter of β-Ga_2O_3 NWs is about 500 nm.[49]

In this paper, the growth process of nanowires is a specific process through a vapor–solid (VS) process; that is, in the absence of any liquid phase, the precursor material is directly deposited on the substrate by gas and becomes a solid under high-temperature heating.[51,52] In the present growth mechanism, no additional metallic catalysts are involved, and a liquid Ga droplet is believed to be a self-catalyst for the growth of β-Ga_2O_3 ribbons. So, we termed the process a self-catalyst growth. The schematic diagram of the nanowire network's growth mechanism is shown in Fig. 3a. After the precursor material (Ga_2O_3 powder) is heated to the target temperature, Ga or Ga_2O vapor will be generated. Next, the generated Ga and Ga_2O vapor rush along with the gas flow and then reached the substrate by the gas carrier. Then, Ga and Ga_2O react synchronously with the rest of oxygen to form condensed clusters, then crystallize and nucleate. As the temperature increases, the vapor pressure continues to increase with the temperature. A VS mechanism will drive highly anisotropic β-Ga_2O_3 NWs growth. When the supersaturated vapor pressure in the tube increases to higher than the equilibrium vapor pressure of the cylindrical sidewall of NWs, growth will begin. Finally, due to lattice mismatch, several one-dimensional β-Ga_2O_3 nanowires are formed. As time goes by, the nanowires stretch and widen and connect to
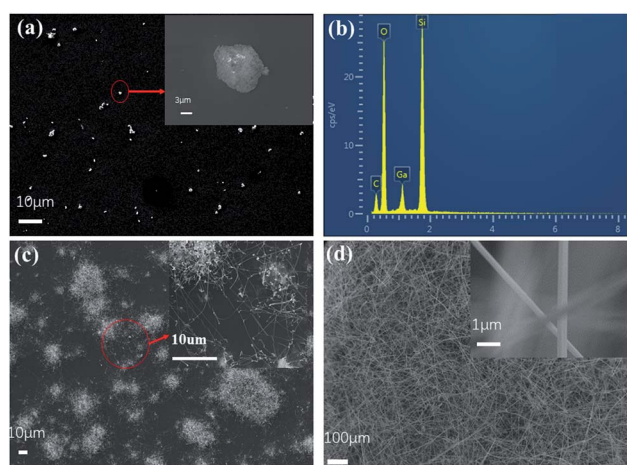

Fig. 2 High magnification SEM image of the β-Ga_2O_3 sample grown at 1150 °C, the insets magnify nanowire networks. (a) 1 minute, inset is a magnification of particles; (c) 5 minutes; (d) 15 minutes; (b) the EDS spectrum of particle in (a).
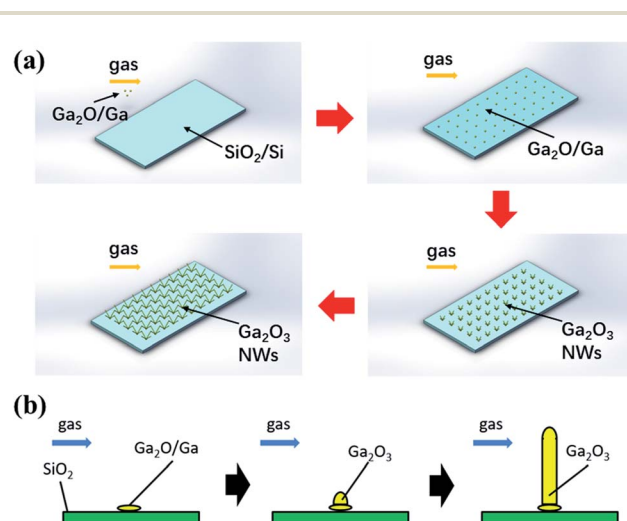

Fig. 3 The schematic diagram of the (a) β-Ga_2O_3 nanowire networks; (b) single β-Ga_2O_3 nanowire.

form a network. Eqn (1)–(4) describe the specific reaction process:[53]

$$Ga_2O_3(S) + 2C(S) \rightarrow Ga_2O(V) + 2CO(g) \tag{1}$$

$$Ga_2O_3(S) + 3C(S) \rightarrow 2Ga(V) + 3CO(g) \tag{2}$$

$$Ga_2O(V) + 2O_2(S) \rightarrow Ga_2O_3(S) \tag{3}$$
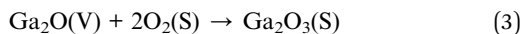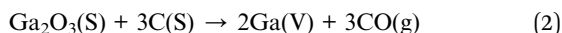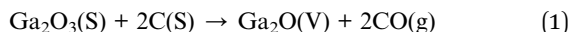
$$4Ga(S) + 3O_2(S) \rightarrow 2Ga_2O_3(S) \tag{4}$$

Fig. 3b shows a schematic diagram of the nanowires self-catalyst grown *via* VS process at high temperature, where Ga/Ga$_2$O nanoparticles deposited on the top of the substrate and induce the further growth of nanowires. At higher temperatures, the high vapor pressure of Ga/Ga$_2$O could induce supersaturation around the catalyst droplet (Ga/Ga$_2$O droplet) quickly, resulting in the formation of a large-size catalyst droplet, which is the reason for self-catalyst growth.[51] In these grown Ga$_2$O$_3$ nanowires, surface diffusion transport and direct nucleation of species from the vapor phase dominate nanowire growth. Faster surface diffusion transport and direct nucleation of species from the vapor phase could significantly enhance the growth of nanowires. In this growth method that used nano-diamond as carbon sources, more Ga/Ga$_2$O could be reduced simultaneously. Therefore, it is the reason why this method can grow longer and thicker nanowire networks in a short time.

To check its photoelectrical performance, β-Ga$_2$O$_3$ nanowires network directly grown on SiO$_2$/Si substrate in 15 minutes is fabricated for the photoelectrical device. A typical metal–semiconductor–metal structure photodetector with internal space around 2 mm between two Ag electrodes is shown Fig. 4a, with Ag metal electrodes are made on the nanowires network by using silver paste paint in Fig. S6.† A measurement of spectral response of the photodetector from 245 nm to 600 nm wavelength was performed. The device has remarkable spectral response in the band less than 280 nm wavelength, especially around 265 nm wavelength, but almost no response in the wavelength which is larger than 400 nm. The deep ultraviolet (DUV)/visible rejection ratio R_{250}/R_{400} is about 1.45×10^3 at 10 V bias is shown in the Fig. S5.† Fig. 4b illustrates the *I–V* characteristics of the photodetector in the dark, under light illumination of 254 nm and 365 nm with a bias of ±6 V. It is evident that the current under 254 nm illumination is much higher than that of non-illumination and 365 nm, which means the 254 nm illumination could significantly enhance the conductivity of the nanowires network device. Besides, the β-Ga$_2$O$_3$ NWs network photodetector was non-sensitive to 365 nm illumination. The dark current is around 4.17×10^{-11} A, and the light current is around 4.45×10^{-7} A, and the on–off ratios (I_{254nm}/I_{dark}) are about 10^3. The *I–V* diagram showed an asymmetric curve because of the formation of Schottky contacts between β-Ga$_2$O$_3$ NWs and Ag. Fig. 4c and d show *I–T* characteristics of photodetector under 6 V bias. The responsivity (R_λ) is defined as the ratio of the response current to the illumination power on photodetector as given by:[11]

$$R_\lambda = \frac{I_{ph} - I_{dark}}{P_0 A} \tag{5}$$

where I_{ph} is the photocurrent, I_{dark} is the dark current, P_0 is the optical power density, and A is the effective illumination area. The responsivity of β-Ga$_2$O$_3$ is 0.38 A W^{-1}. The external quantum efficiency (EQE) η_λ is defend as the number of charge carriers generated per number of incident photons on the device as given by:[54]

$$\eta_\lambda = \frac{1.239R}{\lambda(\mu m)} \tag{6}$$

where λ is the wavelength of the incident light. Associated with the above equation, $\eta_\lambda = 185.4\%$ could be obtained. Fig. 4e and f displays the photoresponse of β-Ga$_2$O$_3$ NW networks photodetector. The dependence of both rising and decay of photocurrent on time can be investigated by using the second-order decay function as follows:

$$y_0 = A_1 e^{t/t_1} + A_2 e^{t/t_2} \tag{7}$$

$$t_r = A_1 t_{r1} + A_2 t_{r2} \tag{8}$$

$$t_d = A_1 t_{d1} + A_2 t_{d2} \tag{9}$$

where t_1 and t_2 are time constants of fast and slow processes, A_1 and A_2 are their relative weight factors, respectively, y_0 also is a constant. t_{r1} and t_{r2} are the time constants of fast and slow current in the rising process; t_{d1} and t_{d2} are the time constants of fast and slow current in the decay process. Under the effect of 254 nm light, the rise time t_r and decay time t_d is 3.01 s and 0.12 s, respectively.

It is well agreed that the chemisorption/desorption of oxygen molecules rules photo response processes in the β-Ga$_2$O$_3$ NWs network. Fig. 5a reveals the adsorption/desorption of oxygen molecules during the DUV response and recovery processes in the β-Ga$_2$O$_3$ NWs. Eqn (10)–(12) describe the specific reaction process:[55]
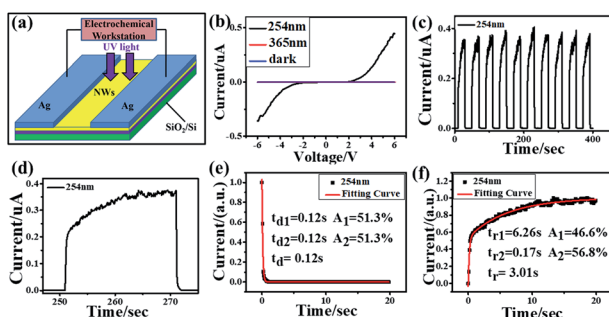

Fig. 4 The device schematic and the photo response characterization (a) the schematic diagram of the β-Ga$_2$O$_3$ UV photodetector; (b) *I–V* characteristics of β-Ga$_2$O$_3$ nanowires network photodetector in a dark condition, under 365 nm and 254 nm light irradiation, respectively; (c) *I–T* characteristics of β-Ga$_2$O$_3$ nanowires network photodetector under 6 V bias with 254 nm light irradiation; (d–f) relationship between the rise/decay time and normalized current of β-Ga$_2$O$_3$ nanowires network photodetector.
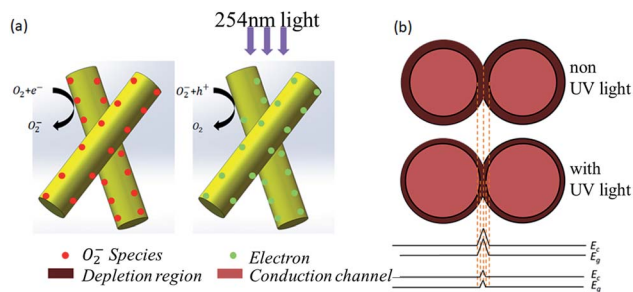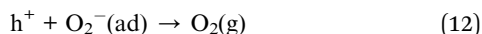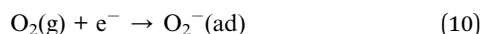
Fig. 5 (a) Schematic of carrier generation; (b) NW–NW junction barrier for electron transfer in the NW network device.

$$O_2(g) + e^- \rightarrow O_2^-(ad) \tag{10}$$

$$hv \rightarrow e^- + h^+ \tag{11}$$

$$h^+ + O_2^-(ad) \rightarrow O_2(g) \tag{12}$$

The oxygen gas molecules adsorbed on the surface of β-Ga_2O_3 NW to form O_2^- by capturing free electrons from β-Ga_2O_3 NW surface (eqn (10)), creating a highly resistive depletion layer near the β-Ga_2O_3 NW surface; Under UV illumination, electron–hole pairs are generated (eqn (11)), the holes transport to the β-Ga_2O_3 NW surface and neutralize the O_2^-, desorbing the oxygen from the β-Ga_2O_3 NW surface (eqn (12)). This hole-capturing process increases the free-carrier concentration, producing an apparent enhancement in conductivity. When the UV irradiation is switched off, holes recombine with electrons, and oxygen molecules are re adsorbed on the β-Ga_2O_3 NW surface by capturing electrons, which increases the resistance of the β-Ga_2O_3 NW again. The resistance of two crossed NWs is dominated by the NW–NW junction barrier instead of the resistance of the NWs themselves. In our β-Ga_2O_3 NW network photodetectors, the electrons must overcome the NW–NW junction barrier during the transfer process.[53] As discussed above the Fig. 5b, the depletion layer can be narrowed by UV illumination due to an increase in carrier density, which is equivalent to a decrease in low barrier height, to pass through the NW network easily upon UV illumination.

Conclusions

In conclusion, the self-catalyst β-Ga_2O_3 nanowire networks on an insulating substrate were synthesized rapidly *via* a catalyst-free and straightforward CVD method. The wide bandgap of the NWs indicates their potential use as efficient UV photodetectors, and their large bandgap of 4.67 eV makes them potential candidates for deep UV detection applications requiring high wavelength selectivity. Simultaneously, the shape changes of the β-Ga_2O_3 nanowires during the growth process were explored. The diameter of the nanowires can grow from 100 nm to 1 μm. The principle and process of autocatalytic growth are briefly explained. The NWs network devices developed in this work showed a ratio (10^3) of light current to dark current, and response and recovery times (within 3.01 s and 0.12 s,

respectively), and the external quantum efficiency (EQE) is about 185.4% under 254 nm DUV light illumination, which could be attributed to their NW–NW junction barrier-dominant conductance. This value of on–off ratio is not lower than that of β-Ga_2O_3 photodetector reported by other researchers. The procedures described in this work can be readily extended to other metal oxide nanomaterials for fabricating large area nanoscale electronics through the bottom up process by reducing electrical artefact and reducing the cost of production.

Conflicts of interest

There are no conflicts to declare.

Acknowledgements

Notes and references

1 H. Chen, K. Liu, L. Hu, A. A. Al-Ghamdi and X. Fang, *Mater. Today*, 2015, **18**, 493–502.
2 L. Sang, M. Liao and M. Sumiya, *Sensors*, 2013, **13**, 10482–10518.
3 E. Monroy, F. Omnes and F. Calle, *Semicond. Sci. Technol.*, 2003, **18**, R33–R51.
4 Y. A. Zou, Y. Zhang, Y. M. Hu and H. S. Gu, *Sensors*, 2018, **18**, 2072.
5 T. Oshima, T. Okuno, N. Arai, N. Suzuki, H. Hino and S. Fujita, *Jpn. J. Appl. Phys.*, 2009, **48**, 011605.
6 Z. Y. Xu and B. M. Sadler, *IEEE Commun. Mag.*, 2008, **46**, 67–73.
7 G. Chen, Z. Xu, H. Ding and B. M. Sadler, *Opt. Express*, 2009, **17**, 3929–3940.
8 M. Razeghi and A. Rogalski, *J. Appl. Phys.*, 1996, **79**, 7433–7473.
9 H. W. Song, L. X. Yu, S. Z. Lu, T. Wang, Z. X. Liu and L. M. Yang, *Appl. Phys. Lett.*, 2004, **85**, 470–472.
10 X. Han, S. L. Feng, Y. M. Zhao, L. Li, Z. Y. Zhan, Z. Y. Tao, Y. X. Fan, W. Q. Lu, W. B. Zuo and D. J. Fu, *RSC Adv.*, 2019, **9**, 1394–1402.
11 Y. M. Zhao, S. L. Feng, H. T. Jiang, S. Ma, Z. Y. Tao, W. Q. Lu and Y. X. Fan, *Phys. E*, 2019, **107**, 1–4.
12 H. T. Jiang, L. Li, S. L. Feng and W. Q. Lu, *Phys. E*, 2018, **104**, 314–319.

13 H. T. Jiang, S. B. Liu, L. Y. Liang and W. Q. Lu, *RSC Adv.*, 2018, **8**, 28928–28933.

14 Z. Y. Zhan, L. P. Xu, J. N. An, H. J. Du, Z. K. Weng and W. Q. Lu, *Adv. Eng. Mater.*, 2017, **19**, 1700101.

15 H. H. Tippins, *Phys. Rev.*, 1965, **140**, A316–A319.

16 G. C. Hu, C. X. Shan, N. Zhang, M. M. Jiang, S. P. Wang and D. Z. Shen, *Opt. Express*, 2015, **23**, 13554–13561.

17 Z. P. Wu, G. X. Bai, Y. Y. Qu, D. Y. Guo, L. H. Li, P. G. Li, J. H. Hao and W. H. Tang, *Appl. Phys. Lett.*, 2016, **108**, 4166–4168.

18 W. Y. Kong, G. A. Wu, K. Y. Wang, T. F. Zhang, Y. F. Zou, D. D. Wang and L. B. Luo, *Adv. Mater.*, 2016, **28**, 10725–10731.

19 W. Feng, X. Wang, J. Zhang, L. Wang, W. Zheng, P. Hu, W. Cao and B. Yang, *J. Mater. Chem. C*, 2014, **2**, 3254–3259.

20 X. Chen, K. Liu, Z. Zhang, C. Wang, B. Li, H. Zhao, D. Zhao and D. Shen, *ACS Appl. Mater. Interfaces*, 2016, **8**, 4185–4191.

21 L.-H. Zeng, M.-Z. Wang, H. Hu, B. Nie, Y.-Q. Yu, C.-Y. Wu, L. Wang, J.-G. Hu, C. Xie, F.-X. Liang and L.-B. Luo, *ACS Appl. Mater. Interfaces*, 2013, **5**, 9362–9366.

22 S. Oh, C.-K. Kim and J. Kim, *ACS Photonics*, 2018, **5**, 1123–1128.

23 W. Y. Weng, T. J. Hsueh, S.-J. Chang, G. J. Huang and S. C. Hung, *IEEE Trans. Nanotechnol.*, 2011, **10**, 1047–1052.

24 L. Binet and D. Gourier, *J. Phys. Chem. Solids*, 1998, **59**, 1241–1249.

25 S. Geller, *J. Chem. Phys.*, 1960, **33**, 676–684.

26 M. Orita, H. Ohta, M. Hirano and H. Hosono, *Appl. Phys. Lett.*, 2000, **77**, 4166–4168.

27 R. Roy, V. G. Hill and E. F. Osborn, *J. Am. Chem. Soc.*, 1952, **74**, 719–722.

28 X. M. Sun and Y. D. Li, *Angew. Chem., Int. Ed.*, 2004, **43**, 3827–3831.

29 N. Ueda, H. Hosono, R. Waseda and H. Kawazoe, *Appl. Phys. Lett.*, 1997, **70**, 3561–3563.

30 X. Wang, Q. Xu, M. Li, S. Shen, X. Wang, Y. Wang, Z. Feng, J. Shi, H. Han and C. Li, *Angew. Chem., Int. Ed.*, 2012, **51**, 13089–13092.

31 M. Higashiwaki, K. Sasaki, A. Kuramata, T. Masui and S. Yamakoshi, *Appl. Phys. Lett.*, 2012, **100**, 013504.

32 S. J. Pearton, J. Yang, P. H. Cary, F. Ren, J. Kim, M. J. Tadjer and M. A. Mastro, *Appl. Phys. Rev.*, 2018, **5**, 011301.

33 Y. Li, T. Tokizono, M. Liao, M. Zhong, Y. Koide, I. Yamada and J.-J. Delaunay, *Adv. Funct. Mater.*, 2010, **20**, 3972–3978.

34 L. Li, E. Auer, M. Liao, X. Fang, T. Zhai, U. K. Gautam, A. Lugstein, Y. Koide, Y. Bando and D. Golberg, *Nanoscale*, 2011, **3**, 1120–1126.

35 R. Zou, Z. Zhang, Q. Liu, J. Hu, L. Sang, M. Liao and W. Zhang, *Small*, 2014, **10**, 1848–1856.

36 W. Y. Weng, T. J. Hsueh, S. J. Chang, G. J. Huang and S. P. Chang, *IEEE Photonics Technol. Lett.*, 2010, **22**, 709–711.

37 P. Feng, J. Y. Zhang, Q. H. Li and T. H. Wang, *Appl. Phys. Lett.*, 2006, **88**, 153107.

38 C. Xie and F. Yan, *Small*, 2017, **13**, 1701822.

39 T. He, Y. Zhao, X. Zhang, W. Lin, K. Fu, C. Sun, F. Shi, X. Ding, G. Yu, K. Zhang, S. Lu, X. Zhang and B. Zhang, *Nanophotonics*, 2018, **7**, 1557–1562.

40 L. Zhang, X. Xiu, Y. Li, Y. Zhu, X. Hua, Z. Xie, T. Tao, B. Liu, P. Chen, R. Zhang and Y. Zheng, *Nanophotonics*, 2020, **9**, 4497–4503.

41 X. Cao, Y. Xing, J. Li, X. Zhang, T. He, L. Zhang, Y. Ma, K. Xu, J. Zhao, W. Tang and B. Zhang, *J. Phys. D: Appl. Phys.*, 2020, **53**, 305103.

42 M. Kumar, S. Kumar, N. Chauhan, D. S. Kumar, V. Kumar and R. Singh, *Semicond. Sci. Technol.*, 2017, **32**, 085012.

43 J.-S. Li, X.-D. Zhang, X. Cao, K. Xu, L. Zhang, Y.-M. Fan and B.-S. Zhang, *Nanotechnology*, 2020, **31**, 02LT01.

44 W. Q. Lu, C. M. Jiang, D. Caudle, C. L. Tang, Q. Sun, J. J. Xu and J. H. Song, *Phys. Chem. Chem. Phys.*, 2013, **15**, 13532–13537.

45 J. Singh, S. S. Patil, M. A. More, D. S. Joag, R. S. Tiwari and O. N. Srivastava, *Appl. Surf. Sci.*, 2010, **256**, 6157–6163.

46 H.-D. Li, H. Lu, D.-D. Sang, D.-M. Li, B. Li, X.-Y. Lue and G.-T. Zou, *Chin. Phys. Lett.*, 2008, **25**, 3794–3797.

47 P. P. He, S. L. Feng, S. Y. Liu, Q. K. Li, J. W. Qi, Z. Y. Zhan, X. Li, Z. H. Li, J. Shen and W. Q. Lu, *RSC Adv.*, 2015, **5**, 105288–105291.

48 S. L. Guo, S. Kang, S. L. Feng and W. Q. Lu, *J. Phys. Chem. C*, 2020, **124**, 4764–4771.

49 I. D. Hosein, M. Hegde, P. D. Jones, V. Chirmanov and P. V. Radovanovic, *J. Cryst. Growth*, 2014, **396**, 24–32.

50 B. Alhalaili, R. J. Bunk, H. Mao, H. Cansizoglu, R. Vidu, J. Woodall and M. S. Islam, *Sci. Rep.*, 2020, **10**, 21434.

51 M. Kumar, V. Kumar and R. Singh, *Nanoscale Res. Lett.*, 2017, **12**, 184.

52 L. W. Sun, M. L. Zhao, F. Wang, W. Jiang, J. Y. Guo, J. T. Li and J. Dai, *J. Nanosci. Nanotechnol.*, 2020, **20**, 2395–2401.

53 X. C. Wu, W. H. Song, W. D. Huang, M. H. Pu, B. Zhao, Y. P. Sun and J. J. Du, *Chem. Phys. Lett.*, 2000, **328**, 5–9.

54 L. Li, H. T. Jiang, X. Han, Z. Y. Zhan, H. J. Du, W. Q. Lu, Z. J. Li, Z. Y. Tao and Y. X. Fan, *Ceram. Int.*, 2017, **43**, 15978–15985.

55 S. Ma, S. L. Feng, S. Kang, F. Wang, X. Fu and W. Q. Lu, *Electron. Mater. Lett.*, 2019, **15**, 303–313.